

Supporting Information

Precise measurement of trapping and manipulation properties of focused fractional vortex beams

Binjie Gao,^a Jisen Wen,^b Guiyuan Zhu,^a Linhua Ye,^a and Li-Gang Wang^{a,}*

^aZhejiang Province Key Laboratory of Quantum Technology and Device and
Department of Physics, Zhejiang University, Hangzhou 310027, China.

^bResearch Center for Intelligent Chips and Devices, Zhejiang Lab,
Hangzhou 311121, China.

* E-mail address of corresponding author: lgwang@zju.edu.cn

1. **Videos of the microparticles trapped before, at, after the focal plane of the objective lens by the FVBs with a half-integer topological charge.**

As a supplement to Figs. 2(a-c) in the main text of the manuscript, the videos show the different trapping effects of the FVBs with a half-integer TC $\alpha = 5.5$ when the trapped microparticles are located before, at, after the focal plane of the objective lens. The position of the particles moves gradually from the position before the focal plane (noted by z -axis position with negative sign) to the focal plane (noted by $z = 0$), then to the position after the focal plane (noted by z -axis position with positive sign). The movement in the z direction is realized by an electric control platform. As shown in the videos, at the back focal plane of the objective lens, a suitable number of particles will usually be captured and rotated to form a circle. However, when the position of the particles is away from the focal plane, the rotation is hard to maintain due to a considerably wide and low-intensity gap, which consists of a series of vortices. As examples, in the videos, when the particles are at the position after the focal plane ($z = +6\mu\text{m}$), the low-intensity gap is on the left side, which hinders the rotation of the particles. When the particle is at the position before the focal plane ($z = -6\mu\text{m}$), the low-intensity line is on the right side, which blocks the rotation of the particles. Fig. S1 is a typical snapshot of the video.

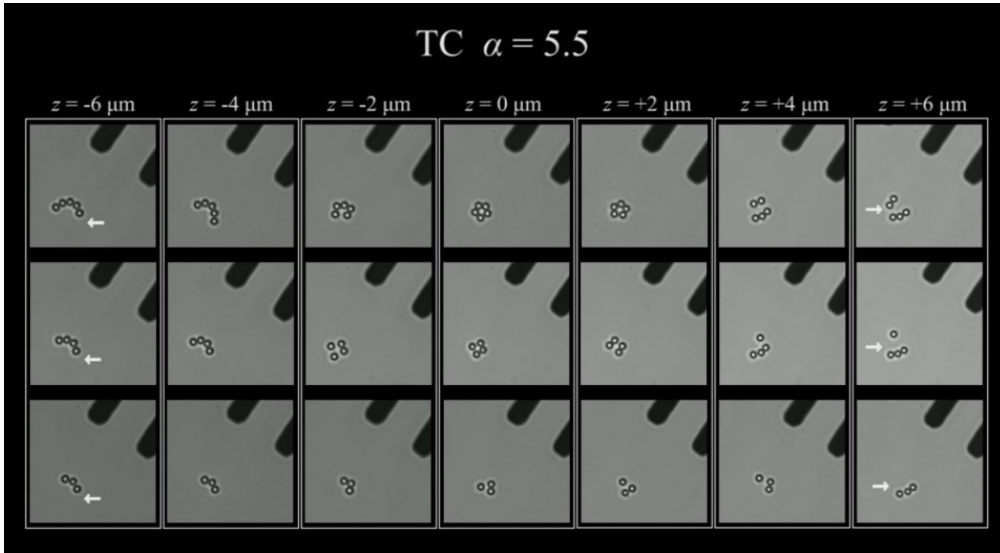


Figure. S1. A typical snapshot of the video in the supplemental material (the video is attached to this supplemental material). The trapping effects of different numbers $N = 3, 4, 5$ of particles trapped before, at, after the focal plane of the objective lens are shown in the videos. The input laser power is fixed at $P = 20 \pm 0.2$ mW and the radius of the microparticle is $a_p = 0.5$ μm . Note that the striped shadow on the upper right is a scale mark of 10 μm on the top glass slide.

2. **Videos of the microparticles trapped in the FVBs with different topological charges.**

As a supplement to Fig. 2(d) in the main text of the manuscript, the videos of the particles' motion are also uploaded in this supplemental material. These videos are the sources of the positions $x(t)$ and $y(t)$ of the particles in Fig. 2(d) in the manuscript. Fig. S2 is a typical snapshot of the video in the supplemental material. For the convenience of observation, we have slowed down the

videos 10 times here, but note that the real duration of particles' movements is limited to 3 seconds for avoiding the big size of the file. In Fig. S2, the first and second rows are the videos that 3 and 5 particles are trapped in the FVBs with different topological charges α . The input laser power is fixed at $P = 20 \pm 0.2$ mW and the radius of the microparticle is $a_p = 0.5$ μm . We can also provide all videos of the trapped microparticles for $N = 3, 4, 5$ from $\alpha = 5.0$ to $\alpha = 7.0$ with an increasing step of 0.1 upon reasonable request.

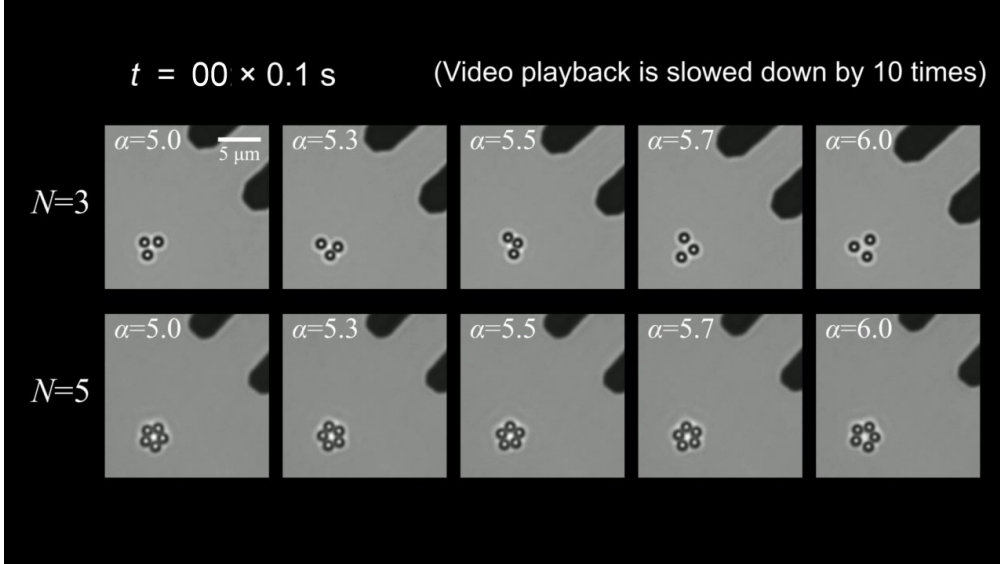


Figure. S2. A typical snapshot of the video in the supplemental material (the video is attached to the supplemental material). The input laser power is fixed at $P = 20 \pm 0.2$ mW and the radius of the microparticle is $a_p = 0.5$ μm . Note that the striped shadow on the upper right is a scale mark of 10 μm on the top glass slide.

3. Videos of a yeast trapped at the focal plane in the FVBs with different topological charges.

As a supplement for the manipulation of microorganisms by the FVBs, we have captured and rotated a yeast using FVBs with different TCs. The videos are also uploaded in the supplemental material. Fig. S3 shows a typical snapshot of the videos. As shown in the videos, FVBs trap could be used to trap and rotate the yeast. However, due to the larger size and the more complicated internal cell structure of the yeast compared with the microspheres, the rotation speed of the yeast is relatively slow. In order to observe more obvious rotational motion, we used a relatively high power (roughly 40 mW) of FVBs to capture the yeast, but this also makes the yeast slightly deformed due to thermal damage (choosing an infrared wavelength laser beam with less absorption by the cells should reduce the thermal damage), which makes it difficult to continue to observe for a long time. Therefore, we captured two yeast cells at the TC region from $\alpha = 5.0$ to 6.0 and from $\alpha = 6.0$ to 7.0 respectively.

The rotation speeds of the yeast trapped in FVBs with different TCs are different. Therefore, as long as the cell's deformation caused by the thermal damage is reduced, the precise control of the cell's rotation speed can be achieved by adjusting the topological charge of FVBs. This further

demonstrated the continuous manipulation on the bio-objects by using FVBs.

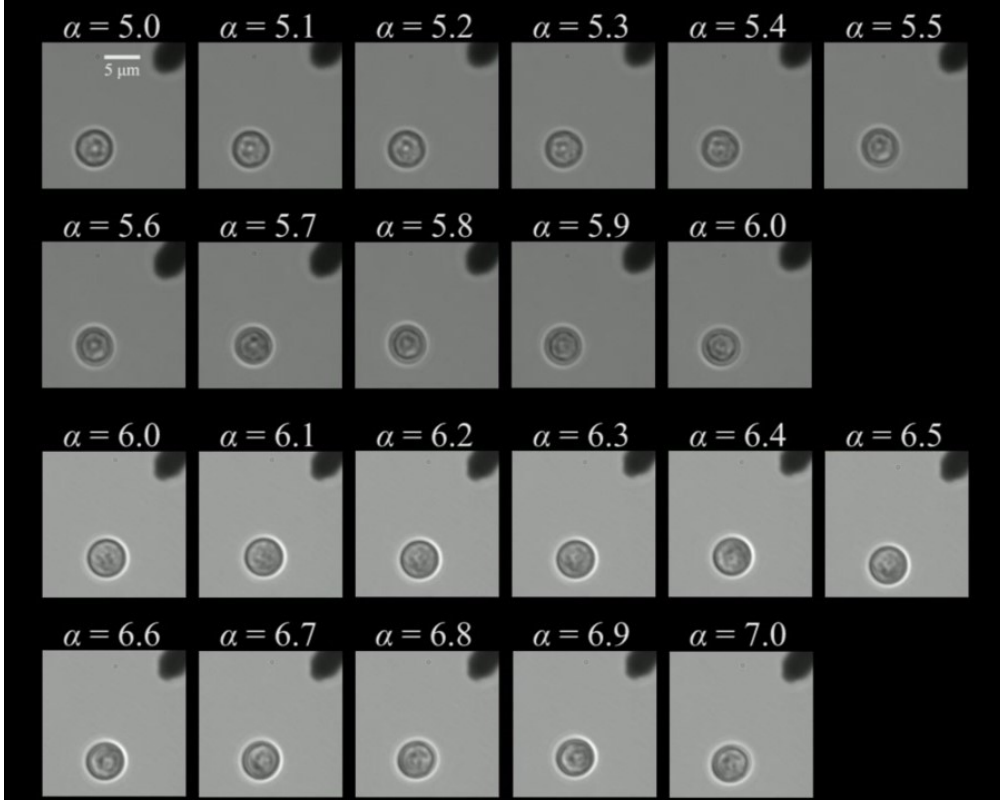


Figure. S3. A typical snapshot of the video in the supplemental material (the video is attached to the supplemental material). The first two rows and the last two rows are videos of two different yeasts captured in FVBs with TC from $\alpha = 5.0$ to 6.0 and from $\alpha = 6.0$ to 7.0 , respectively. The input laser power is fixed at $P = 40$ mW and the diameter of the yeasts is roughly $5 \mu\text{m}$. Note that the striped shadow on the upper right is a scale mark on the top glass slide.

4. Examples of calculated intensity distribution, Poynting vector of focused FVBs by using the tight-focusing theory and the experimentally measured intensity distribution of focused FVBs.

As a supplement to the Figs. 2 and 4 in the manuscript, the numerically calculated the intensity distributions of FVBs with several different α before, at, and after the focal plane using the tight-focusing theory^{1,2} are shown in Fig. S4. The intensity rings in the angular direction have a much larger gap and more inhomogeneous when the trapped plane is moved away from the focal plane. That is similar to trapping properties in Figs. 2(a)-2(c) in the manuscript, at the focal plane the particles are rotated much easier than the situations away from the focal plane. The simulated parameters are the same as the experiment, with beam waist $w_0 = 2\text{mm}$, numerical aperture $\text{NA} = 1.25$ for an oil immersion objective lens, and the focal length of the objective lens $f = 2\text{mm}$.

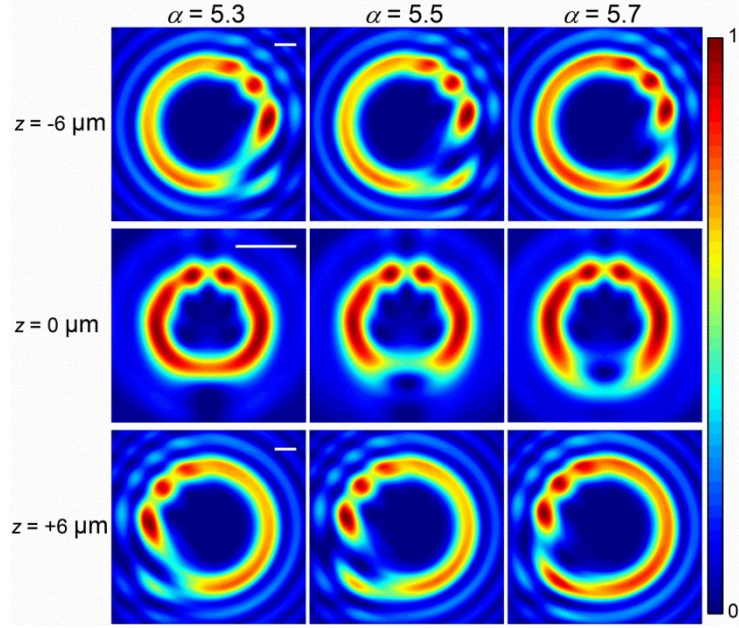


Fig. S4. The calculated intensity distributions of FVBs with different TCs before ($z = -6 \mu\text{m}$), at ($z = 0 \mu\text{m}$), after ($z = +6 \mu\text{m}$) the focal plane by using the tight-focusing theory.^{1,2} The simulation parameters are consistent with the experiment. The parameters are chosen as $\lambda = 532\text{nm}$, $w_0 = 2\text{mm}$, $f = 2\text{mm}$, $\text{NA} = 1.25$. White scale bar, $1.0 \mu\text{m}$.

In Fig. S5, we provided the calculated intensity distributions and the transverse Poynting vector at the focal plane of the focused FVBs using the tight-focusing theory.¹⁻³ As shown in Fig. S5, there is a vortex darkness crossing the intensity ring when fractional topological charge α is slightly larger than half integers. From Figs. S5(a) and (c), the intensity-gradient force provides the radial trapping force, which makes multiple particles form a necklace shape under a suitable number. Meanwhile, as shown in Figs. S5(b, d), the magnitude of \vec{S}_{\perp} roughly maintains a circular shape except when α is close to half integers. Thus the transverse scattering force in the angular direction drives the radial trapped particles. In the cases of a single particle trapped in the focused FVBs, the inhomogeneous gradient force may hinder the rotation, however as the number of particles increases the collision between particles transferring the OAM of focused FVBs overcome the mentioned hindering effect.

In Fig. S6, we provided the measured intensity distributions at the focal plane of the objective lens according to Ref. 4 by replacing the glass sample room with a reflection mirror in our experimental setup. The experimental intensity distribution is considerably good consistent with the calculated intensity distribution based on the tight-focusing theory in Figs. S5(a) and (c).

Both the numerically calculated and measured intensity distributions (see the Figs. S5 and S6) illustrate that when α is roughly near $\alpha = 5.7$ and 6.7 , a vortex darkness is nested in the intensity ring and the ring of transverse Poynting vector, then such hindering effect is nearly the strongest. It almost consistent with the experimental result that the minimum value of the average trap stiffness between two integer TCs appears near $\alpha = 5.6$ or 5.7 and $\alpha = 6.6$ or 6.7 in Fig. 4(b) in our manuscript.

Besides, it is also worth pointing out that the experimental intensity distribution in Fig. S6 is

not perfectly uniform even for the integer vortex beams, which is due to the fact that the practical fundamental beam emitted from our solid-state laser is not perfect circular symmetry, but with a slight ellipticity. However, because the collision between multiple microparticles trapped in the focal plane of FVBs can overcome the hindering effect of the intensity ripples, the rotation can keep well even for FVBs in our experiment.

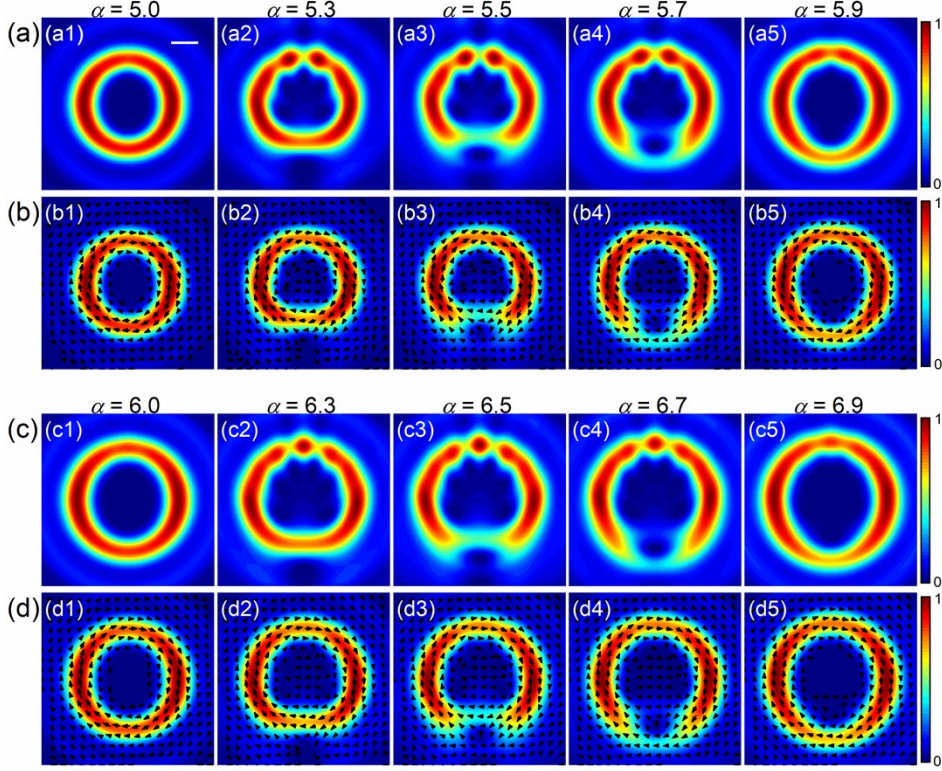


Figure. S5. (a, c) Numerical intensity distribution and (b, d) the transverse Poynting vector \vec{S}_{\perp} at the focal plane of FVBs by using the tight focusing theory based on the Debye vector integral.¹⁻³ The index numbers 1-5 in subfigures are the different cases of α . The magnitude of the \vec{S}_{\perp} is denoted by color bar and its direction is denoted by the black arrows. The magnitudes of the intensity and the transverse Poynting vector are normalized. The simulation parameters are consistent with the experiment. White scale bar, 0.5 μm .

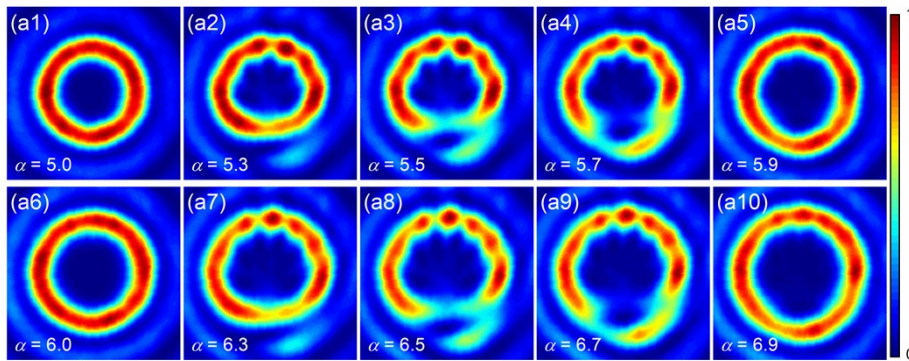


Figure. S6. Experimentally measured intensity distribution at the focal plane of the FVBs by replacing the glass sample room with a reflection mirror in our experimental setup.⁴ Subfigures (a1-a10) show the intensity distribution of focused FVBs with different TCs α . The magnitude of the intensity is normalized.

5. Additional data of the experimental power spectra for the trapped microspheres in the FVBs with TCs $\alpha = 6.0, 6.2, 6.4, 6.5, 6.7, 6.9$.

As a supplement to Fig. 4 in the main text of the manuscript, Fig. S7 shows the experimental power spectra for the trapped microspheres in the fractional vortex beams with different TCs $\alpha = 6.0, 6.2, 6.4, 6.5, 6.7, 6.9$. The value of the trap stiffness κ derived from the fitting curve of the r direction power spectrum can be found in Fig. 4(b) in the manuscript.

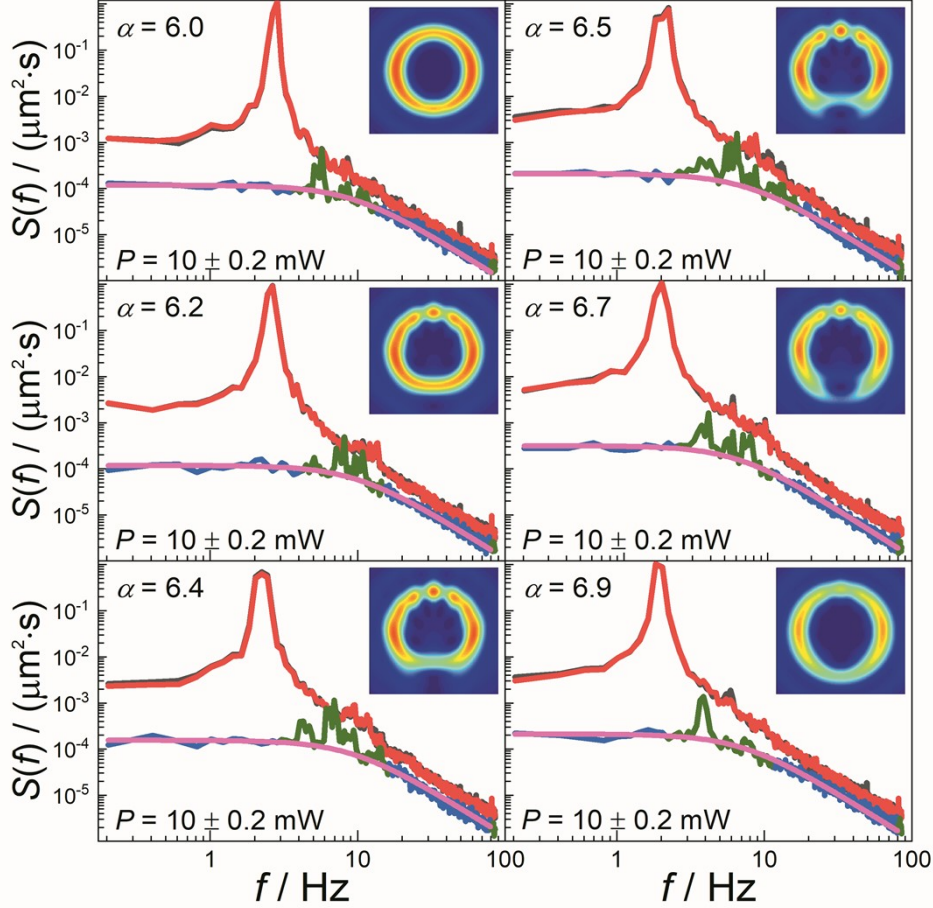


Figure. S7. Experimental power spectra for the trapped microspheres in the FVBs with different TCs $\alpha = 6.0, 6.2, 6.4, 6.5, 6.7, 6.9$. Different power spectra obtained from the different data for $x(t)$, $y(t)$, and $r(t)$ are, respectively, denoted by the black, red, and blue solid lines. The black and red solid lines are almost overlapped. The fitting curve of the power spectrum for the component $r(t)$ is depicted by a thick-solid pink line, and the green region for high-order harmonic peaks is neglected during fitting. The insets are the energy-normalized theoretical intensity distributions of the FVBs at the back focal plane of the objective lens.

6. Videos of the smaller microparticles ($a_p = 0.25 \mu\text{m}$) trapped before, at, after the focal plane of the objective lens by the FVBs with a half-integer TC.

In Supplemental Video 4, five smaller microparticles with radius of $0.25 \mu\text{m}$ are trapped at the position before, at, and after the focal plane of the objective lens, respectively. Fig. S8 is a typical snapshot of the Video 4. In order to suppress the Brownian motion of smaller particles in liquid, the input power now increases to be $P = 50 \text{ mW}$. Compared with the situation in our manuscript

with the microparticle's radius of $0.5 \mu\text{m}$, it's observed that the rotation of smaller microparticles trapped at the focal plane is uneven. One is due to the fact that the particle size is smaller than the intensity breakpoint, which makes it harder to cross. Another factor is that five microparticles with radius of $0.25 \mu\text{m}$ are still not formed into a necklace shape in this situation.

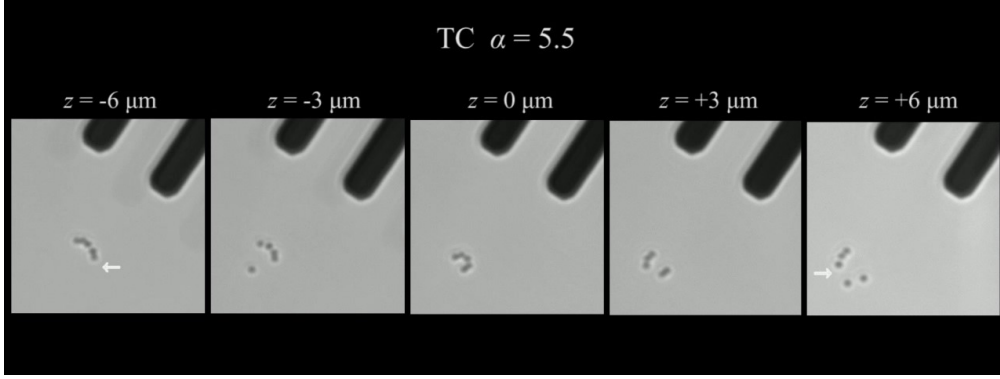


Figure. S8. A typical snapshot of the Video 4 in the supplemental material (the video is attached to this supplemental material). The trapping effects of five microparticles trapped before, at, after the focal plane of the objective lens are shown in the videos. The input laser power is fixed at $P = 50 \text{ mW}$. Note that the radius of the microparticle used here is $a_p = 0.25 \mu\text{m}$. The striped shadow on the upper right is a scale mark of $10 \mu\text{m}$ on the top glass slide.

7. Videos of the smaller microparticles ($a_p = 0.25 \mu\text{m}$) trapped in the FVBs with different TCs.

In Supplemental Video 5, there are eight microparticles with radius of $0.25 \mu\text{m}$ trapped in focused FVBs with the same input power $P = 50 \text{ mW}$ in Video 4. The Topological charge is increasing from 5.0 to 7.0. And the videos that the microparticles trapped at the position before, at, and after the focal plane of the objective lens are provided in Video 5. Fig. S9 is a typical snapshot of the Video 5. In this case, eight microparticles nearly form a necklace shape at the focal plane of FVBs again. As the number of the particles increases, we can see again that the interaction (collision) among the rotating particles pushes the particles across the intensity breakpoint. This Video 5 is similar to Fig. 2 in our manuscript. From these videos, it's seen that when the trapped plane is close to the focal plane of FVBs, under the suitable number of microparticles forming a necklace shape, the collective rotation can keep well even at half integers. Furthermore, it's observed that the focused FVBs in the focal plane for the smaller-sized microparticles can be used to rotate particles much easier than that in the non-focal plane. But for smaller microparticles, one needs to increase the laser input power to overcome the influence of the Brownian motion of microparticles in liquid.

However, due to the limitation of the resolution of our current microscopic system, we didn't do further experiments on much smaller nanoparticles with radius smaller than $0.25 \mu\text{m}$.

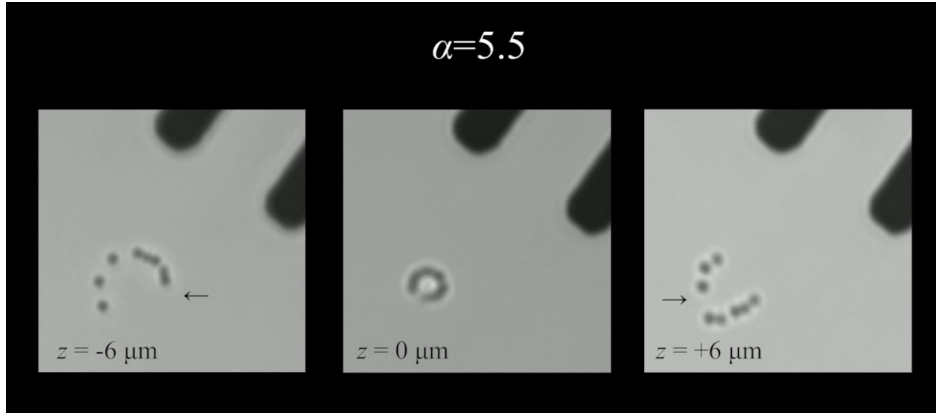


Figure. S9. A typical snapshot of the Video 5 in the supplemental material (the video is attached to this supplemental material). The trapping effects of eight microparticles trapped before, at, after the focal plane of the objective lens with varying TCs are shown in the videos. The Topological charge is increasing from 5.0 to 7.0. The input laser power is fixed at $P = 50$ mW. Note that the radius of the microparticle used here is $a_p = 0.25$ μm . The striped shadow on the upper right is a scale mark of 10 μm on the top glass slide.

References

1. B. Richards and E. Wolf, Electromagnetic diffraction in optical systems, II. Structure of the image field in an aplanatic system, *Proc. R. Soc. Lond. A*, **253**(1274), 358–379 (1959).
2. Z. Chen, J. Pu, and D. Zhao, Tight focusing properties of linearly polarized Gaussian beam with a pair of vortices, *Physics Letters A*, **375**(32), 2958–2963 (2011).
3. L. Allen, M. W. Beijersbergen, R. J. C. Spreeuw, and J. P. Woerdman, Orbital angular momentum of light and the transformation of Laguerre-Gaussian laser modes, *Phys. Rev. A*, **45**(11), 8185–8189 (1992).
4. Y. Roichman, I. Cholis, and D. G. Grier, Volumetric imaging of holographic optical traps, *Opt. Express*, **14**(22), 10907 (2006).